

# Energy Detection for MIMO Decision Fusion in Underwater Sensor Networks

Pierluigi Salvo Rossi, *Senior Member, IEEE*, Domenico Ciuonzo, *Member, IEEE*,  
Torbjörn Ekman, *Member, IEEE*, and Hefeng Dong, *Member, IEEE*

**Abstract**—In this paper, we study the performance of the energy detector when considered for binary hypothesis decision fusion in underwater acoustic wireless sensor networks with a multiple-access reporting channel. Energy detection is appealing in terms of computational complexity and limited system knowledge requirements, i.e., channel state information, signal-to-noise ratio, and local performance of the sensors are not needed at the receiver side, then the interest for performance assessment over underwater acoustic channels arises. Here, we demonstrate that energy detection may be applied with good results to underwater sensor networks. The impact on the performance of various design parameters is considered, including sampling frequency, number of transmitting sensors, and number of receiving elements (hydrophones).

**Index Terms**—Decision fusion, energy detection, multiple-input multiple-output (MIMO), underwater sensor networks.

## I. INTRODUCTION

UNDERWATER sensor networks represent the solution for many different applications ranging from environmental monitoring and data collection to survey missions and coastal surveillance, from aquaculture to remote control in offshore oil industry [1]. One of the major challenges is the effective use of the underwater acoustic channel, which is characterized by time-varying extended multipath due to the acoustic propagation mechanism in water [2]. As a consequence of the limited coherence bandwidth, which is both frequency and range dependent, inter-symbol interference (ISI) is very common

Manuscript received September 29, 2014; accepted October 21, 2014. Date of publication October 23, 2014; date of current version January 9, 2015. This work was supported in part by the ERCIM within the Alain Bensoussan Fellowship Program, in part by the Project entitled Embedded Systems within the Research Framework Networks of Excellence through the POR Campania FSE 2007/2013, Italy, and in part by the Faculty of Information Technology, Mathematics and Electrical Engineering, Norwegian University of Science and Technology, Trondheim, Norway, through the CAMOS Project. The associate editor coordinating the review of this paper and approving it for publication was Dr. Thilo Sauter.

P. Salvo Rossi is with the Department of Industrial and Information Engineering, Second University of Naples, Caserta 81100, Italy, and also with the Department of Electronics and Telecommunications, Norwegian University of Science and Technology, Trondheim 7491, Norway (e-mail: salvorossi@ieee.org).

D. Ciuonzo is with the Department of Electrical Engineering and Information Technology, University of Naples Federico II, Naples 80138, Italy (e-mail: domenico.ciuonzo@ieee.org).

T. Ekman and H. Dong are with the Department of Electronics and Telecommunications, Norwegian University of Science and Technology, Trondheim 7491, Norway (e-mail: torbjorn.ekman@iet.ntnu.no; hefeng.dong@iet.ntnu.no).

Color versions of one or more of the figures in this paper are available online at <http://ieeexplore.ieee.org>.

Digital Object Identifier 10.1109/JSEN.2014.2364856

in underwater communication systems [3]. Additionally, the time-varying nature of the environment induces large Doppler shifts into the transmitted signals [4].

The availability of an effective model for underwater acoustic channels is desirable for system design. However, modeling of underwater acoustic channels is still an open issue. Statistical models, including both small-scale and large-scale effects, have been proposed to match real-world data from various locations (see [5], [6], and references therein), but no general consensus has been reached yet. Robustness with respect to channel behavior is an extremely valuable feature for an underwater system.

## A. Underwater Acoustic Communications and Networking

The need for high-data-rate systems has mainly motivated the design and the analysis of advanced techniques at the physical layer in underwater scenarios such as channel equalization, coherent modulation, iterative decoding, multi-input multi-output (MIMO) processing, multicarrier transmission, multichannel decision feedback, phase conjugation [7]–[13]. Underwater MIMO communications are considered in [14], where a point-to-point MIMO communication is implemented in a shallow-water frequency-selective channel through the use of space-time coding and decision feedback equalizer. Furthermore, a linear soft-input soft-output equalizer is developed in [15] for turbo-equalization of a point-to-point MIMO scenario with Alamouti encoding at transmit side and its effectiveness is assessed through both simulated and real-world data. Differently, in [16] a spatial modulation technique is developed in order to exploit multiple parallel channels arising from rich-scattering underwater environments, thus leading to both increased data-rate and received power (validation through experimental data). A thorough study of the spatial processing gain in relationship to the number of receivers, the receiver separation and the array aperture is presented in [17], with focus on the performance of both diversity combining and beamforming algorithms.

Networking technologies and their applicability to underwater acoustic networks have been considered in [18]. Spread-spectrum-based medium access control with high throughput, low delay and low energy consumption has been proposed in [19]. Energy-efficient multiple-access protocols suited for scenarios with long and unknown propagation delays were proposed and analyzed in [20]–[22]. Planning of

underwater sensor networks for data collection has been investigated in [23] focusing on how the quality of the communication channels impacts on the overall performance, while optimal sensor placement taking into account the time dynamic of the underwater environment has been considered in [24]. The differences in energy consumption between underwater acoustics and terrestrial radio apparatuses are explored in [25], and energy-efficient routing protocols for WSNs have been tailored for underwater acoustic scenarios in [26] and [27]. Frequency and power allocation strategies for multi-hop underwater sensor networks were designed in [28]. Approaches combining routing and node replacement were considered to deal with long lifetime requirements in sensor networks for monitoring applications [29].

### B. Decision Fusion

Decision fusion denotes collective processing of informations coming from various sensors for a final assessment on a binary hypothesis test. Referring to (more traditional) electromagnetic wave propagation in free space, wireless sensor networks have been studied from many different points of view during the last decades in various research contexts. Distributed detection through a wireless sensor network is still an active area for research: the typical scenario considers many sensors that transmit their local decisions to a fusion center which takes a (hopefully more reliable) global decision by appropriately combining the received information.<sup>1</sup> Several works (see [30]–[32]) have considered architectures based on parallel access channels: each sensor has a non-interfering dedicated (i.e. orthogonal to the others) channel to communicate with the fusion center. Near-optimal fusion rules with full channel state information (CSI) available at the receiver have been discussed in [33].

Recently, there has been an interest in exploiting the interfering nature of wireless media in presence of multiple transmitters and/or receivers for distributed-detection tasks [34]–[36]. More specifically, various solutions based on MIMO techniques have been investigated and compared in terms of performance, complexity, and knowledge requirements [37]. Analytical results for an effective system operating at low SNR are presented in [38]. Finally, a very simple receiver based on energy detection has been proven to be optimal (under Bayesian/Neyman-Pearson frameworks) in Rayleigh fading channels [39]. Additionally, relaxation of the perfect coherent detection assumptions and related system design is found in [40], while the impact of coexistence of multiple interfering sensor networks is considered in [41].

Decision fusion has been studied in underwater networks [42] where scan statistic is exploited for active detection. However, the sensor architecture was still relying on a parallel access channel. To the best of our knowledge, *MIMO decision fusion in underwater scenarios is still unexplored.*

### C. Contribution and Organization of the Paper

In this paper we consider energy detection for MIMO decision fusion in underwater acoustic channels.

<sup>1</sup>We focus on centralized architectures. However, decentralized architectures for distributed detection have also received large interest in the literature.

Distributed underwater sensors transmit a signal if an event of interest is detected locally, i.e. we are assuming on-off keying (OOK) modulation. An array receiver fuses the signals from the multiple sensors using energy detection, i.e. the energy received from multiple sensors is the statistics for the binary decision on the occurrence of an event in the region monitored by the network. We assume a binary source, making the work suitable for applications such as threshold-based event detection.

It is worth mentioning that [43] compares, in the context of distributed detection, OOK with frequency shift keying (FSK). It is shown that OOK exhibits error performance comparable to that of FSK in addition to energy saving, however the work assumes parallel channels to the fusion center, while our work focuses on interfering channels.

For typical underwater acoustic channels, on one hand the optimal rule for decision fusion is not practical (as in most scenarios), on the other hand the fusion rule based on energy detection is suboptimal due to the fact that the channel statistics do not match the Rayleigh fading model.<sup>2</sup> Here we analyze the impact on the performance of various design parameters such as: SNR, pulse duration, sampling frequency, integration time, number of transmitting sensors, number of receiving elements (hydrophones), and sensor quality. Also, we show a reasonable setup can approach the optimum performance in a realistic scenario. The *main advantages* of the presented system are:

- it does not require perfect synchronization;
- it does not require either channel estimation for instantaneous CSI or statistical CSI;
- it does not require knowledge of either local sensor performance or SNR;
- it is energy efficient, as it employs OOK;
- it achieves excellent performance, even with low-quality sensors.

It is worth mentioning that the energy detector is quite insensitive to Doppler effects, which typically severely degrade performance of underwater communication systems. These features make it appealing for applications of interest in the oil industry such as undersea oilfields monitoring. Furthermore, underwater sensor networks are usually based on short-range low-power communications, and along this line we stress that OOK modulation is energy efficient if one of the two hypotheses is significantly less probable than the other (this is common in monitoring applications for anomaly detection) [34]. In this work we do not make any assumption on the dynamic of the source as we do not exploit any possible time correlation of the source at the receiver. This issue falls beyond the scope of this paper and will be explored in future works.

The outline of the paper is the following: in Sec. II we present the system model under investigation; we describe the statistics for the decision at the fusion center and the figures

<sup>2</sup>According to [39] and the decision fusion literature, we mean that the channel coefficients of the equivalent discrete-time model presented in the following are not complex-valued zero-mean Gaussian. Differently, according to [6] and the underwater acoustics literature, it is worth noticing that Rayleigh fading is often used to denote the statistics of each single path, then the considered channel would be named Rayleigh according to such a definition.

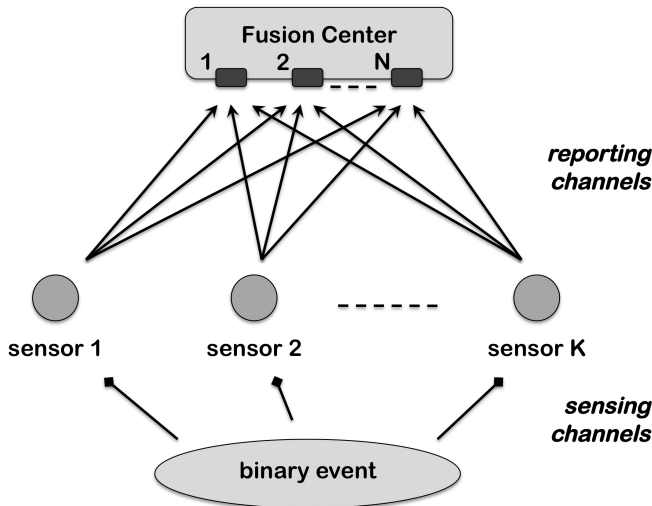


Fig. 1. Scenario for collaborative binary decision with  $K$  sensors and one fusion center equipped with  $N$  hydrophones.

for system performance in Sec. III; Sec. IV highlights and compares the performance of simulated systems with different setups; finally Sec. V gives some concluding remarks.

*Notation:* Lower-case bold letters denote vectors, with  $a_n$  denoting the  $n$ th element of  $\mathbf{a}$ ; upper-case bold letters denote matrices, with  $A_{n,m}$  denoting the  $(n,m)$ th element of  $\mathbf{A}$ ;  $\mathbf{I}_N$  denotes the  $N \times N$  identity matrix;  $\mathbf{0}_N$  denotes the  $N$ -length vector whose elements are 0;  $\delta(\cdot)$  denotes the Dirac function;  $\mathbb{E}\{\cdot\}$ ,  $(\cdot)^t$ , and  $\|\cdot\|$  denote expectation, transpose, and Frobenius norm operators;  $(\mathbf{A}_1^t, \dots, \mathbf{A}_N^t)^t$  denotes the vertical concatenation of  $N$  matrices;  $\Pr(\mathcal{A})$  denotes the probability of the event  $\mathcal{A}$ ;  $p(a)$  denotes the probability density function of the random variable  $a$ ;  $\lfloor a \rfloor$  denotes the largest integer value smaller than or equal to  $a$ ;  $\Re(a)$  and  $\Im(a)$  denote the real and imaginary parts of  $a$ , respectively;  $j$  is the imaginary unit;  $\mathcal{A}^n$  denotes the  $n$ th Cartesian power of the set  $\mathcal{A}$ ;  $\sim \mathcal{N}_{\mathbb{C}}(\boldsymbol{\mu}, \boldsymbol{\Sigma})$  means “distributed according to a proper complex normal distribution with mean  $\boldsymbol{\mu}$  and covariance  $\boldsymbol{\Sigma}$ ”; a baseband signal  $a(t)$  is associated to a bandpass signal  $\tilde{a}(t) = \Re(a(t) \exp(j2\pi f_c t))$  with  $f_c$  denoting the carrier frequency.

## II. SYSTEM MODEL

As shown in Fig. 1, we consider the scenario in which  $K$  sensors sense autonomously the environment, each taking a local decision concerning a binary hypothesis test. The two hypotheses are denoted  $\mathcal{H}_0$  and  $\mathcal{H}_1$  and the corresponding a-priori probabilities  $\pi_0$  and  $\pi_1$ , respectively.

We assume that the local sensing and decision process by the  $k$ th sensor is fully described by the local probability of false alarm ( $p_f(k)$ ) and the local probability of missed detection ( $p_m(k)$ ), both assumed to be stationary and conditionally independent given the specific hypothesis. We will denote *homogeneous scenario* the special case in which local performance (i.e. the local probabilities of false alarm and missed detection) are identical for each sensor (in this case the dependence on  $k$  is omitted and they will be denoted  $p_f$  and  $p_m$ ). Sensors, each with one single acoustic

transducer (projector), communicate quasi-simultaneously<sup>3</sup> their decision to a fusion center, equipped with  $N$  hydrophones, whose aim is to provide a robust decision on the basis of the multiple received information. All the sensors employ the same binary modulation: for energy saving purposes we consider OOK modulation, with identical parameters (transmission pulse, carrier frequency, etc.).

### A. Analog Signal Model

The signal transmitted by the  $k$ th sensor is

$$\tilde{s}_k(t) = \Re(x_k g(t) \exp(j2\pi f_c t)), \quad (1)$$

where  $g(t)$  is the baseband pulse<sup>4</sup> with duration  $T_p$ , and  $x_k \in \mathcal{X} = \{0, 1\}$  represents the binary information encoding the local decision (we assume 0 for  $\mathcal{H}_0$  and 1 for  $\mathcal{H}_1$ ).

The reporting channels, connecting the sensors to the fusion center, are both dispersive and noisy. More specifically, the impulse response of the channel between the projector of the  $k$ th sensor and the  $n$ th hydrophone at the fusion center is modeled as

$$h_{n,k}(t; \tau) = \sum_{\ell=1}^L \alpha_{\ell}^{(n,k)}(t) \delta(\tau - \tau_{\ell}^{(n,k)}(t)), \quad (2)$$

i.e. we consider a time-varying multipath channel where:  $\alpha_{\ell}^{(n,k)}(t)$  is the attenuation of the  $\ell$ th path at time  $t$  on the  $(n,k)$ th link,  $\tau_{\ell}^{(n,k)}(t)$  is the delay of the  $\ell$ th path at time  $t$  on the  $(n,k)$ th link, and  $L$  is the maximum number of resolvable paths over all the set of  $N \times K$  links. This model is also referred to as *multiscale multilag channel model* in [5] and represents a good candidate for wideband underwater acoustic channels. We will consider the two following assumptions (as in [7]–[9]):

- (i) the amplitudes are constant within one or more transmissions, i.e.  $\alpha_{\ell}^{(n,k)}(t) = \alpha_{\ell}^{(n,k)}$ ;
- (ii) the delays are expressed in the form  $\tau_{\ell}^{(n,k)}(t) = \tau_{\ell}^{(n,k)} - \phi_{\ell}^{(n,k)} t$ , where  $\tau_{\ell}^{(n,k)}$  is the initial delay and  $\phi_{\ell}^{(n,k)}$  is the Doppler rate, i.e. the ratio between the relative speed of transmitter/receiver and the speed of sound.

Finally, Gaussian noise with flat power spectral density within the receiver bandwidth is added at the receiver: the noise contribution at the output of the receive filter is denoted  $\tilde{w}_n(t)$ .

Denoting  $\tau_{\max}$  the maximum duration of the channel, the signal received by the  $n$ th hydrophone of the fusion center is then written as

$$\tilde{y}_n(t) = \sum_{k=1}^K \int_0^{\tau_{\max}} h_{n,k}(t; \tau) \tilde{s}_k(t - \tau) d\tau + \tilde{w}_n(t), \quad (3)$$

<sup>3</sup>As perfect synchronization is not required, “quasi-simultaneously” means that signals transmitted from different sensors overlap in time at receiver location: no dedicated channel is required to the single sensor.

<sup>4</sup>For sake of simplicity we include in  $g(t)$  the effects of both transmit and receive filters, i.e. it is the convolution of the corresponding impulse responses. This choice avoids explicit notation for the shape of the transmit and receive filters which is not necessary to the considered analysis.

providing the following baseband representation:

$$y_n(t) = \sum_{k=1}^K \sum_{\ell=1}^L \left[ \alpha_\ell^{(n,k)} e^{-j2\pi f_c \tau_\ell^{(n,k)}} e^{j2\pi f_c \phi_\ell^{(n,k)} t} \right. \\ \left. \times x_k g \left( (1 + \phi_\ell^{(n,k)})t - \tau_\ell^{(n,k)} \right) \right] + w_n(t). \quad (4)$$

It is worth noticing that we assume a sort of coarse synchronization. Although the sensors do not need to be perfectly synchronized (the asynchronism may be included in the channel delay), we assume that the received signal undergoes no ISI from signals related to different (other than the current) sensing operations. In the case of a monitoring application, this means that sensing and transmission are performed in accordance with the duration of the channel impulse response, i.e. the reciprocal of the sensing and transmission rate must be larger than the maximum duration of the channel (which includes the asynchronism of the transmitting sensors).

### B. Discrete-Time Signal Model

After sampling with frequency  $f_s$ , the  $m$ th sample of the received signal is given by

$$y_n[m] = \sum_{k=1}^K H_{n,k}[m] x_k + w_n[m], \quad (5)$$

where  $y_n[m] = y_n(m/f_s)$ ,  $w_n[m] = w_n(m/f_s)$ , and

$$H_{n,k}[m] = \sum_{\ell=1}^L \alpha_\ell^{(n,k)} e^{-j2\pi f_c \tau_\ell^{(n,k)}} e^{j2\pi \frac{f_c}{f_s} \phi_\ell^{(n,k)} m} \\ \times g \left( (1 + \phi_\ell^{(n,k)}) \frac{m}{f_s} - \tau_\ell^{(n,k)} \right), \quad (6)$$

represent the received signal, the noise and the channel coefficient, respectively. Define  $\mathbf{y}[m] = (y_1[m], \dots, y_N[m])^t$  the vector collecting the signals at the  $m$ th sampling time over all  $N$  hydrophones,  $\mathbf{w}[m] = (w_1[m], \dots, w_N[m])^t \sim \mathcal{N}_{\mathbb{C}}(\mathbf{0}_N, \sigma_w^2 \mathbf{I}_N)$  the corresponding noise contribution,  $\mathbf{x} = (x_1, \dots, x_K)^t$  the local decisions from all the  $K$  sensors, and

$$\mathbf{H}[m] = \begin{pmatrix} H_{1,1}[m] & \cdots & H_{1,K}[m] \\ \vdots & \ddots & \vdots \\ H_{N,1}[m] & \cdots & H_{N,K}[m] \end{pmatrix}, \quad (7)$$

the matrix of channel coefficients at the  $m$ th sampling time. Then the discrete-time model for the received signal at the  $m$ th sampling time is

$$\mathbf{y}[m] = \mathbf{H}[m] \mathbf{x} + \mathbf{w}[m]. \quad (8)$$

An integration time  $T_o$ , i.e. collecting signals from  $M = \lfloor f_s T_o \rfloor$  successive sampling times as  $\mathbf{y} = (\mathbf{y}[1]^t, \dots, \mathbf{y}[M]^t)^t$ ,  $\mathbf{w} = (\mathbf{w}[1]^t, \dots, \mathbf{w}[M]^t)^t$ , and  $\mathbf{H} = (\mathbf{H}[1]^t, \dots, \mathbf{H}[M]^t)^t$ , provides the following discrete-time model<sup>5</sup>

$$\mathbf{y} = \mathbf{H} \mathbf{x} + \mathbf{w}. \quad (9)$$

<sup>5</sup>In the following we will consider the effect on system performance of undersampling/oversampling. In this cases, although keeping the same variance, noise samples would exhibit correlation. For sake of simplicity, we will not consider colored noise and assume that the noise contribution ( $\mathbf{w}$ ) is white independently of the sampling frequency ( $f_s$ ).

Channel quality is measured through the ratio between the unitary energy of the active symbol and the noise variance, i.e. we define the link SNR as follows

$$\text{SNR} = \frac{1}{\sigma_w^2}, \quad (10)$$

where we assumed a normalized channel such that  $\mathbb{E}\{\sum_{\ell} (\alpha_\ell^{(n,k)})^2\} = 1$ , i.e. we refer to the (per-link) received SNR in the ergodic sense.

### III. DECISION FUSION

The decision is usually performed as a test comparing a signal-dependent statistic ( $\lambda(\mathbf{y})$ ) and a fixed threshold ( $\gamma$ )

$$\begin{aligned} \hat{\mathcal{H}} &= \mathcal{H}_1 \\ \lambda(\mathbf{y}) &\geq \gamma, \\ \hat{\mathcal{H}} &= \mathcal{H}_0 \end{aligned} \quad (11)$$

where  $\hat{\mathcal{H}}$  denotes the estimated hypothesis. Performance is evaluated in terms of global probability of false alarm ( $q_f$ ) and global probability of missed detection ( $q_m$ ), defined as follows

$$q_f = \Pr(\lambda(\mathbf{y}) > \gamma | \mathcal{H}_0), \quad (12)$$

$$q_m = \Pr(\lambda(\mathbf{y}) < \gamma | \mathcal{H}_1). \quad (13)$$

Another metric of interest is the global probability of error ( $q_e$ ), defined as follows

$$q_e = \pi_0 q_f + \pi_1 q_m. \quad (14)$$

The threshold in Eq. (11) is usually selected in order to minimize the error probability (according to the Bayes criterion [44]) or to ensure a target probability of false alarm (according to the Neyman-Pearson criterion [44]). For system performance evaluation, in this paper we consider the behavior of the global probability of missed detection ( $q_m$ ) versus the global probability of false alarm ( $q_f$ ), commonly denoted *complementary receiver operating characteristic* (CROC).

The log-likelihood ratio (LLR) of the received signal under the two hypotheses provides the optimal test (under both Bayesian/Neyman-Pearson frameworks [44])

$$\begin{aligned} \lambda(\mathbf{y}) &= \log \left( \frac{p(\mathbf{y} | \mathcal{H}_1)}{p(\mathbf{y} | \mathcal{H}_0)} \right) \\ &= \log \left( \frac{\mathbb{E}_{\mathbf{H}} \left\{ \sum_{\mathbf{x} \in \mathcal{X}^K} p(\mathbf{y} | \mathbf{H}, \mathbf{x}) \prod_{k=1}^K \Pr(x_k | \mathcal{H}_1) \right\}}{\mathbb{E}_{\mathbf{H}} \left\{ \sum_{\mathbf{x} \in \mathcal{X}^K} p(\mathbf{y} | \mathbf{H}, \mathbf{x}) \prod_{k=1}^K \Pr(x_k | \mathcal{H}_0) \right\}} \right), \\ &= \log \left( \frac{\sum_{\mathbf{x} \in \mathcal{X}^K} \mathbb{E}_{\mathbf{H}} \left\{ e^{-\frac{\|\mathbf{y} - \mathbf{H}\mathbf{x}\|^2}{\sigma_w^2}} \right\} \prod_{k=1}^K \Pr(x_k | \mathcal{H}_1)}{\sum_{\mathbf{x} \in \mathcal{X}^K} \mathbb{E}_{\mathbf{H}} \left\{ e^{-\frac{\|\mathbf{y} - \mathbf{H}\mathbf{x}\|^2}{\sigma_w^2}} \right\} \prod_{k=1}^K \Pr(x_k | \mathcal{H}_0)} \right). \end{aligned} \quad (15)$$

However, the optimal test is computationally expensive (the complexity is exponential with  $K$ ) and additionally has high knowledge requirements (statistical CSI, SNR and local sensor performance are needed).

In the case of OOK, a common simpler alternative is obtained replacing the LLR with the energy of the received signal, i.e.

$$\lambda(\mathbf{y}) = \|\mathbf{y}\|^2, \quad (16)$$

which apparently requires little computational complexity and also has the advantage that neither CSI nor SNR nor local sensor performance are needed. Such a test has been proved to be optimal in Rayleigh fading scenarios [35], [39]. Nonetheless, in the following section we show how it can be an interesting test also in underwater acoustic channels.

The benchmark for performance evaluation is the *observation bound* [37], i.e. the performance achieved in the ideal case that the reporting channel is perfect. For homogeneous scenarios, the observation bound is computed as follows,

$$q_f = \sum_{\ell=c}^K \binom{K}{\ell} p_f^\ell (1-p_f)^{K-\ell}, \quad (17)$$

$$q_m = \sum_{\ell=0}^{c-1} \binom{K}{\ell} (1-p_m)^\ell p_m^{K-\ell}, \quad (18)$$

where  $c \in \{0, \dots, K\}$  is a discrete threshold. For non-homogeneous scenarios, Eqs. (17) and (18) may be generalized, but the closed-form expression is generally intractable (especially for large  $K$ ) [45].

#### IV. SIMULATION RESULTS

We have simulated various scenarios with MATLAB software. CROC curves have been obtained averaging the results over  $10^4$  Monte Carlo runs. We have considered a biased binary event with a-priori probabilities  $\pi_0 = 0.7$  and  $\pi_1 = 0.3$ . Up to  $K = 40$  transmitting sensors have been considered, whose local sensing performance has been chosen among the following sets:  $p_f \in \{0.01, 0.05, 0.1\}$  and  $p_m \in \{0.1, 0.5\}$ .

Sensors transmit at carrier frequency  $f_c = 10$  kHz and unitary-energy rectangular baseband pulse<sup>6</sup> with duration  $T_p \in \{0.5, 1, 2\}$  ms is assumed. The  $NK$  links among the  $K$  projectors and the  $N$  hydrophones are assumed independent and identically distributed. On each link, channel coefficients have been randomly generated according to the following specifications:

- $L = 10$  discrete resolvable paths with inter-arrival time being exponentially distributed with mean  $\Delta_\tau \in \{0.5, 1, 2\}$  ms; delays assumed statistically independent with respect to the sensors ( $k$ ) while not with respect to the hydrophones ( $n$ ) where delay differences at different hydrophones are generated according to a zero-mean Gaussian distribution with standard deviation  $d/c$  (being  $d = 5$  m the approximate size of the receive array and  $c = 1500$  m/s and the speed of sound in water);
- amplitudes are Rayleigh distributed with average power decreasing exponentially with delay (6 dB over 10 ms);

<sup>6</sup>The use of a rectangular pulse is not realistic (remember that the pulse include the effects of both transmit and receive filters. However, without losing any significant phenomenon affecting system performance, we assume a rectangular pulse for ease of simulation.

TABLE I

LIST OF PARAMETERS CONSIDERED IN THE PRESENTED SIMULATIONS. BOLD-FACE NUMBERS DENOTE THE DEFAULT VALUES

Name	Symbol	Value
num. sensors	$K$	$\{10, \dots, \mathbf{15}, \dots, 40\}$
carrier freq.	$f_c$	$\mathbf{10}$ kHz
pulse duration	$T_p$	$\{0.25, 0.5, \mathbf{1}, 1.5, 2, 2.5, 3\}$ ms
local fal.al. pr.	$p_f$	$\{0.01, \mathbf{0.05}, 0.1\}$
local miss.det. pr.	$p_m$	$\{0.1, \mathbf{0.5}\}$
num. paths	$L$	$\mathbf{10}$
velocity st.dev.	$v$	$\mathbf{1}$ m/s
av. inter-arr. time	$\Delta_\tau$	$\{0.5, \mathbf{1}, 2\}$ ms
num. hydroph.	$N$	$\{\mathbf{1}, \dots, 4\}$
sampling freq.	$f_s$	$\{0.5, \mathbf{1}, 2\}$ kHz
integration time	$T_o$	$\{2.5, 5, \mathbf{10}, 15, 20, 25, 30, 35\}$ ms
SNR	SNR	$\{-30, -\mathbf{20}, -10\}$ dB

- Doppler rates are sampled from a Gaussian distribution with zero mean and standard deviation  $v/c$  (being  $v = 1$  m/s the velocity standard deviation for the scenario<sup>7</sup>).

Up to  $N = 4$  hydrophones are assumed at the fusion center, operating with sampling frequency and integration time chosen among the following sets:  $f_s \in \{0.5, 1, 2\}$  kHz and  $T_o \in \{5, 10, 20\}$  ms. We have considered three different SNRs, i.e.  $\text{SNR} \in \{-30, -20, -10\}$  dB.

Tab. I summarizes the values for the set of parameters considered in the presented simulations, which are similar to those considered in [9], where simulations were paired with experiments in the North Atlantic Ocean at water depth of 15 m and distance from transmitter and receiver elements between 60 m and 1000 m. Unless differently specified, the following “default” parameters are assumed:  $K = 15$  transmitting sensors,  $N = 1$  hydrophone, local performance  $p_f = 0.05$  and  $p_m = 0.5$ , pulse duration  $T_p = 1$  ms, sampling frequency  $f_s = 1$  kHz, integration time  $T_o = 10$  ms,  $\text{SNR} = -20$  dB and average inter-arrival time  $\Delta_\tau = 1$  ms. It is worth noticing that assuming an integration time  $T_o = 10$  ms and negligible asynchronism effects means that the positioning accuracy of the sensors with respect to the fusion center should not exceed a few meters, i.e. much smaller than 15 m, although resynchronization on a regular basis may be needed (e.g. due to sound speed fluctuations).

**SNR:** The impact of the SNR is shown in Fig. 2. It shows the CROC curves obtained in a homogeneous scenario. The obvious improvement with SNR is apparent. In order to assess the sensitivity with respect to the SNR, it is worth noticing that moving from  $\text{SNR} = -20$  dB to  $\text{SNR} = -10$  dB at a global probability of false alarm  $q_f = 0.05$  allows to reduce the global probability of missed detection from  $q_m = 0.099$  to  $q_m = 0.048$ . The operation point of the single sensor, i.e. the local sensing performance ( $p_f, p_m$ ), is also shown in the plot for comparison purpose (depicted with a black asterisk).

**Sampling Frequency and Integration Time:** The joint impact of the sampling frequency ( $f_s$ ) and of the integration time ( $T_o$ ) is shown in Fig. 3. It shows the CROC curves obtained in a

<sup>7</sup>It is related to the velocity of the fusion center and to the velocity of any scatterer in the environment.

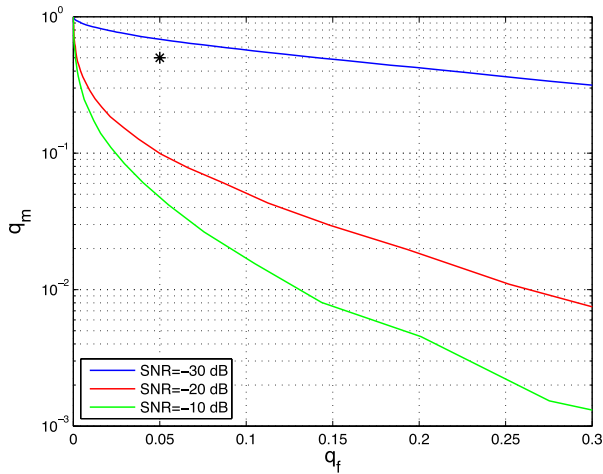


Fig. 2. Impact of the SNR on the CROC. Curves refer to a homogeneous scenario with  $K = 15$  transmitting sensors, each with  $p_f = 0.05$  and  $p_m = 0.5$  and pulse duration  $T_p = 1$  ms, and  $N = 1$  hydrophone at the fusion center, operating with sampling frequency  $f_s = 1$  kHz and integration time  $T_o = 10$  ms. The black asterisk (\*) represents the local sensing performance of the single sensor.

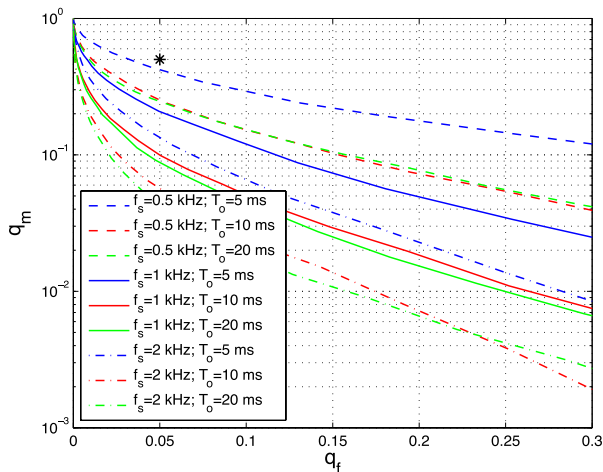


Fig. 3. Impact of the sampling frequency ( $f_s$ ) and of the integration time ( $T_o$ ) on the CROC. Curves refer to a homogeneous scenario with  $K = 15$  transmitting sensors, each with  $p_f = 0.05$  and  $p_m = 0.5$  and pulse duration  $T_p = 1$  ms, and  $N = 1$  hydrophone at the fusion center, operating at SNR =  $-20$  dB. The black asterisk (\*) represents the local sensing performance of the single sensor.

homogeneous scenario. The improvement with  $f_s$  is apparent. Differently, the trend with respect to  $T_o$  is not monotonic: starting from short integration time, we first experience a rapid performance improvement with the duration, and then after an optimal duration is achieved performance slowly degrades. The same behavior has been also confirmed with different choices of the pulse duration. In our opinion, the reason for this phenomenon is the tradeoff between two conflicting phenomena. Increasing  $T_o$  has the positive effect to allow collecting a large portion of the transmitted energy. On the other hand, after most of the links have expired, the benefits from keeping on listening to contributions from other links (not yet expired) are canceled or even dominated by the noise on the expired links. In order to highlight such a behavior, Fig. 4 shows the global probability of missed detection ( $q_m$ )

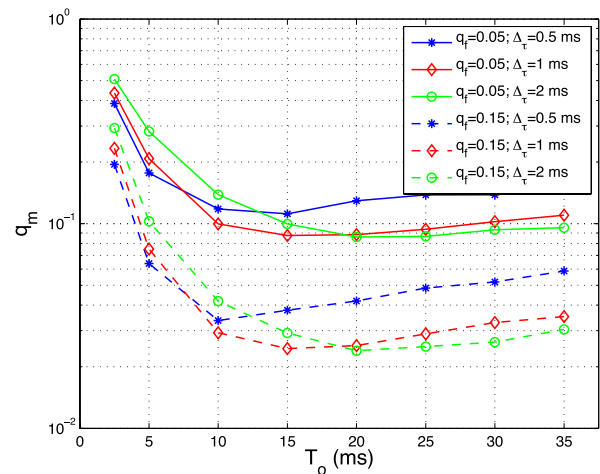


Fig. 4. Impact of the average inter-arrival time ( $\Delta_\tau$ ) and of the integration time ( $T_o$ ) on the global probability of missed detection ( $q_m$ ) assuming a fixed global probability of false alarm ( $q_f = 0.05$  and  $q_f = 0.15$ ). Curves refer to a homogeneous scenario with  $K = 15$  transmitting sensors, each with  $p_f = 0.05$  and  $p_m = 0.5$  and pulse duration  $T_p = 1$  ms, and  $N = 1$  hydrophone at the fusion center, operating with sampling frequency  $f_s = 1$  kHz at SNR =  $-20$  dB.

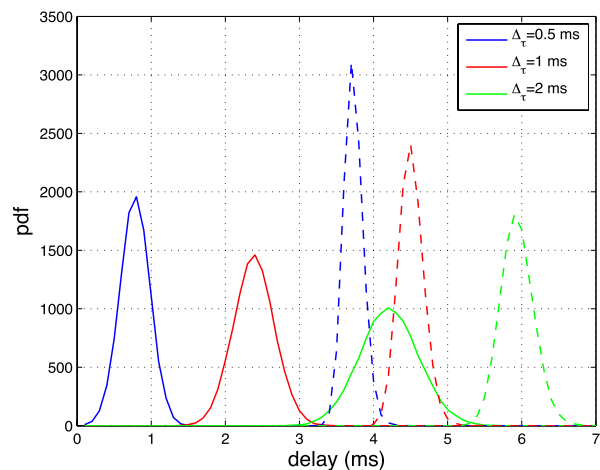


Fig. 5. Impact of the average inter-arrival time ( $\Delta_\tau$ ) on the statistics of the average delay (solid lines) and of the rms delay spread (dashed lines).

vs. the integration time ( $T_o$ ) for the considered scenarios when the global probability of false alarm is fixed ( $q_f = 0.05$  and  $q_f = 0.15$ ). Three different values of average inter-arrival time ( $\Delta_\tau$ ) are considered with the corresponding empirical probability density function (pdf) of the average delay ( $\tau_\mu$ ) and root mean square delay spread ( $\tau_{rms}$ ), defined as in [46], shown in Fig 5. Various simulations have confirmed that the optimum value of the integration time is approximately found as  $T_o \approx \tau_\mu + 3\tau_{rms}$ . It is worth mentioning that the non-monotonic behavior of the performance with respect to the integration time confirms the fact that the energy detector is not optimal in underwater acoustic channels, *as adding uninformative measurements can even degrade the performance*. Also, having Rayleigh channel statistics is crucial for the derivation of the optimality of the energy detection (see [39]). In order to assess the sensitivity with respect to the sampling frequency ( $f_s$ ), it is worth noticing that moving from

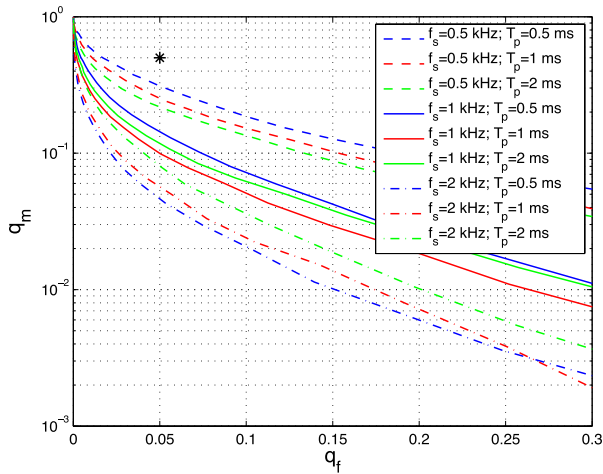


Fig. 6. Impact of the sampling frequency ( $f_s$ ) and of the pulse duration ( $T_p$ ) on the CROC. Curves refer to a homogeneous scenario with  $K = 15$  transmitting sensors, each with  $p_f = 0.05$  and  $p_m = 0.5$ , and  $N = 1$  hydrophone at the fusion center, operating at  $\text{SNR} = -20$  dB and integration time  $T_o = 10$  ms. The black asterisk (\*) represents the local sensing performance of the single sensor.

$f_s = 0.5$  kHz to  $f_s = 1$  kHz and then to  $f_s = 2$  kHz at a global probability of false alarm  $q_f = 0.05$  and with an integration time  $T_o = 10$  ms allows to reduce the global probability of missed detection from  $q_m = 0.25$  to  $q_m = 0.099$  and then to  $q_m = 0.057$ .

**Sampling Frequency and Pulse Duration:** The joint impact of the sampling frequency ( $f_s$ ) and of the pulse duration ( $T_p$ ) is shown in Fig. 6. It shows the CROC curves obtained in a homogeneous scenario. Again, the improvement with  $f_s$  is apparent, while (analogously to the behavior with respect to  $T_o$ ) the trend with respect to  $T_p$  is not monotonic: starting from short pulse duration, we first experience a performance improvement with the duration, and then after an optimal duration is achieved performance degrades. The same behavior has been also confirmed with different choices of the integration time. In our opinion, the reason for this phenomenon is again the tradeoff between two conflicting phenomena. Increasing  $T_p$  has the positive effect to allow reducing the silent intervals during the observation interval (remember that the channel response is creating different replicas of the transmitted pulse, each with different attenuation, delay and compression/expansion). However, with unitary-energy constraint, increasing the pulse duration makes each replica more vulnerable to the noise until it is completely masked by the noise level. In order to highlight such a behavior, Fig. 7 shows the global probability of missed detection ( $q_m$ ) vs. the pulse duration ( $T_p$ ) for the considered scenarios when the global probability of false alarm is fixed ( $q_f = 0.05$  and  $q_f = 0.15$ ). The corresponding empirical pdf of the discrete-time-model channel amplitudes ( $|H_{n,k}|$ ) are shown in Fig. 8: channels behave as a hybrid random variable with a Rayleigh-distributed continuous component and a discrete component located in 0 representing the silent intervals.<sup>8</sup>

<sup>8</sup>In Fig. 8, the impulses are meant to be located in 0. They are instead located on different negative values for visibility. Also, their area has been divided by 10 in the figure in order to stay within the same range of the continuous part and improve readability of the figure.

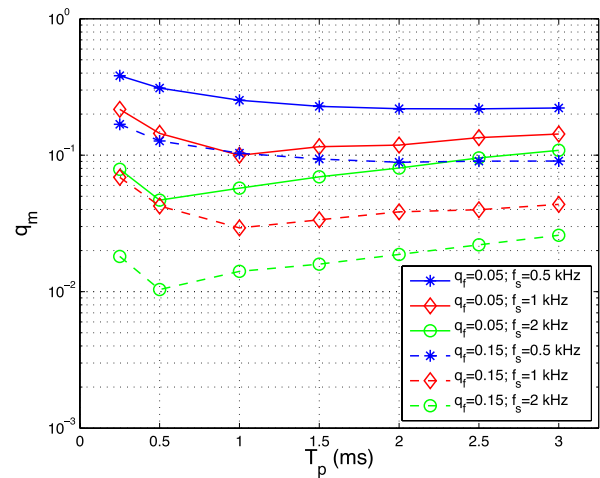


Fig. 7. Impact of the sampling frequency ( $f_s$ ) and of the pulse duration ( $T_p$ ) on the global probability of missed detection ( $q_m$ ) assuming a fixed global probability of false alarm ( $q_f = 0.05$ ). Curves refer to a homogeneous scenario with  $K = 15$  transmitting sensors, each with  $p_f = 0.05$  and  $p_m = 0.5$ , and  $N = 1$  hydrophone at the fusion center, operating at  $\text{SNR} = -5$  dB and integration time  $T_o = 10$  ms. The black asterisk (\*) represents the local sensing performance of the single sensor.

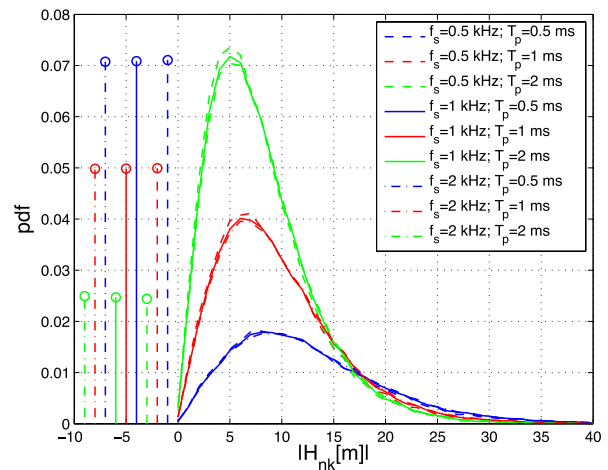


Fig. 8. Impact of the sampling frequency ( $f_s$ ) and of the pulse duration ( $T_p$ ) on the statistics of the discrete-time model channel coefficients.

Various simulations have confirmed that the optimum value of the pulse duration is found as  $T_p = 1/f_s$ . It is worth noticing how the beneficial effect of the channel statistics when increasing the pulse duration is confirmed as the impulse area decreases (i.e. the silent intervals vanish) and the statistics approach a Rayleigh distribution.

**Number of Sensors and Hydrophones:** The impact of the number of transmitting sensors ( $K$ ) and of the number of hydrophones ( $N$ ) is shown in Fig. 9. It shows the CROC curves obtained in a homogeneous scenario. The improvement with both  $K$  and  $N$  is apparent. In order to assess the sensitivity with respect to  $K$ , it is worth noticing that moving from  $K = 10$  to  $K = 15$  at a global probability of false alarm  $q_f = 0.05$  and with  $N = 1$  hydrophone at the fusion center allows to reduce the global probability of missed detection from  $q_m = 0.19$  to  $q_m = 0.099$ . In order to assess the sensitivity with respect to  $N$ , it is worth noticing that moving from  $N = 1$  to  $N = 2$  hydrophones at a global probability of

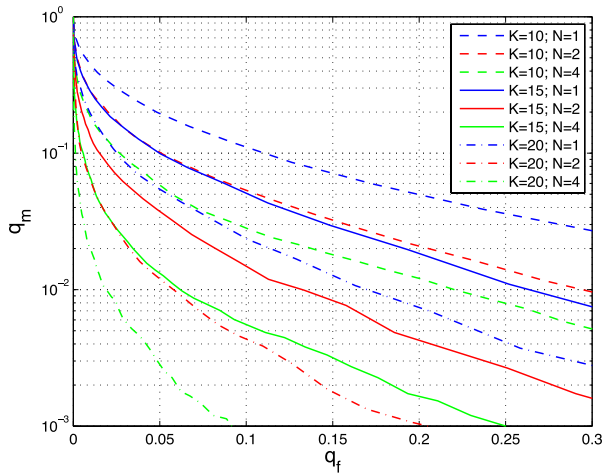


Fig. 9. Impact of the number of transmitting sensors ( $K$ ) and of the number of hydrophones ( $N$ ) on the CROC. Curves refer to a homogeneous scenario: sensors have  $p_f = 0.05$  and  $p_m = 0.5$  and pulse duration  $T_p = 1$  ms, and fusion center operates at SNR =  $-10$  dB with sampling frequency  $f_s = 1$  kHz and integration time  $T_o = 10$  ms. The black asterisk (\*) represents the local sensing performance of the single sensor.

false alarm  $q_f = 0.1$  in a system with  $K = 15$  transmitting sensors allows to reduce the global probability of missed detection from  $q_m = 0.099$  to  $q_m = 0.037$ .

In addition, it is worth noticing that the spatial diversity of the system is  $NK$ , i.e. the number of individual links. However, systems with the same product  $NK$  but different values for  $K$  and  $N$  undergo different performance, usually with the system having larger  $K$  and smaller  $N$  performing better. This should be related to the different amount of noise at the receiver on one hand, while on the other hand to the fact that missed detections make the number of active sensors less than  $K$  and then a larger  $K$  would balance the negative impact of missed detection on the system. Additionally, due to saturating effects (usually SNR-dependent and becoming more relevant with increasing  $K$  and/or  $N$ ), general conclusions on the considered scenario cannot to be drawn.

**Local Performance:** The impact of the local sensor performance ( $p_f$  and  $p_m$ ) is shown in Fig. 10. It shows the CROC curves obtained in a homogeneous scenario. The improvement with both  $p_f$  and  $p_m$  is apparent. In order to assess the sensitivity with respect to  $p_f$ , it is worth noticing that moving from  $p_f = 0.1$  to  $p_f = 0.05$  (with fixed  $p_m = 0.5$ ) at a global probability of false alarm  $q_f = 0.05$  allows to reduce the global probability of missed detection from  $q_m = 0.25$  to  $q_m = 0.099$ . In order to assess the sensitivity with respect to  $p_m$ , it is worth noticing that moving from  $p_m = 0.5$  to  $p_m = 0.1$  (with fixed  $p_f = 0.05$ ) at a global probability of false alarm  $q_f = 0.05$  allows to reduce the global probability of missed detection from  $q_m = 0.099$  to  $q_m = 0.0035$ .

**Optimal vs. Energy Detection:** The performance loss of energy detection with respect to optimal detection<sup>9</sup> for

<sup>9</sup>Actually, the curves related to the optimal detector have been obtained using the Max-Log approximation in Eq. (15). Such a detector, namely Max-Log detector, has been shown to perform very close to the optimal detector without suffering of numerical instability due to the presence of exponential functions with large dynamic range [37].

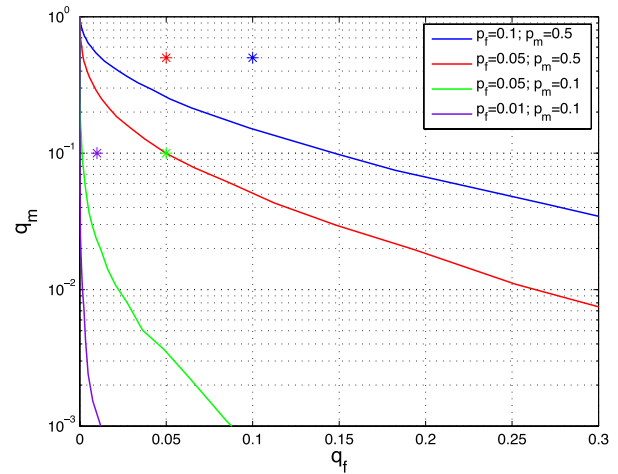


Fig. 10. Impact of the local sensor performance ( $p_f$  and  $p_m$ ) on the CROC. Curves refer to a homogeneous scenario with  $K = 15$  transmitting sensors, each with pulse duration  $T_p = 1$  ms, and  $N = 1$  hydrophone at the fusion center, operating at SNR =  $-20$  dB with sampling frequency  $f_s = 1$  kHz and integration time  $T_o = 10$  ms. The asterisks (\*) represent the local sensing performance of the single sensor (associated to the corresponding curve through color).

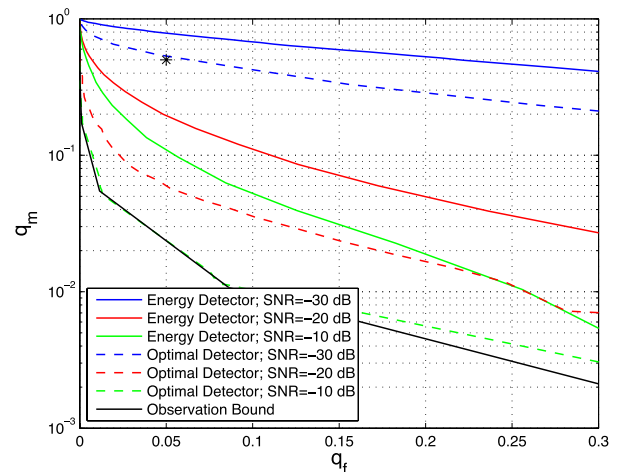


Fig. 11. Performance loss of the energy detector with respect to the optimal detector. Curves refer to a homogeneous scenario with  $K = 10$  transmitting sensors, each with  $p_f = 0.05$  and  $p_m = 0.5$  and pulse duration  $T_p = 1$  ms, and  $N = 1$  hydrophone at the fusion center, operating with sampling frequency  $f_s = 1$  kHz and integration time  $T_o = 10$  ms. The black asterisk (\*) represents the local sensing performance of the single sensor.

different SNRs is shown in Fig. 11. It shows the CROC curves obtained in a homogeneous scenario with  $K = 10$  transmitting sensors. The (ideal) observation bound is also shown for complete comparison. In order to assess the gap, it is worth noticing that energy and optimal detectors at a global probability of false alarm  $q_f = 0.05$  and SNR =  $-20$  dB provide a global probability of missed detection of  $q_m = 0.19$  and  $q_m = 0.059$ , respectively.

**Approaching the Observation Bound:** Fig. 12 shows the same CROC curves shown in Fig. 2 with two more CROC curves: one is the observation bound for a homogeneous scenario with default parameters, and the other one is the CROC curve in a homogeneous scenario with  $N = 4$

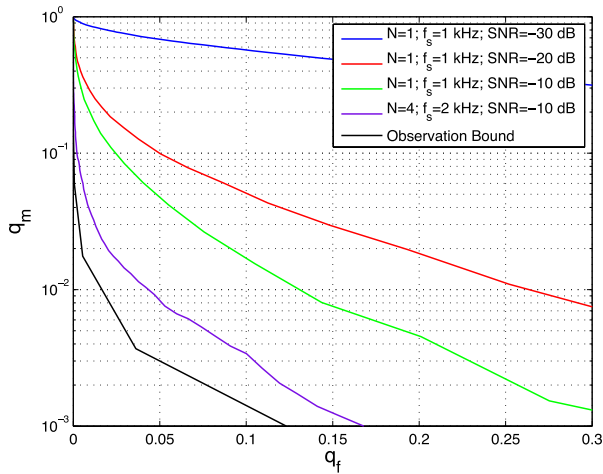


Fig. 12. Approaching the observation bound with  $K = 15$  transmitting sensors, each with  $p_f = 0.05$  and  $p_m = 0.5$  and pulse duration  $T_p = 1$  ms. The integration time is  $T_o = 10$  ms.

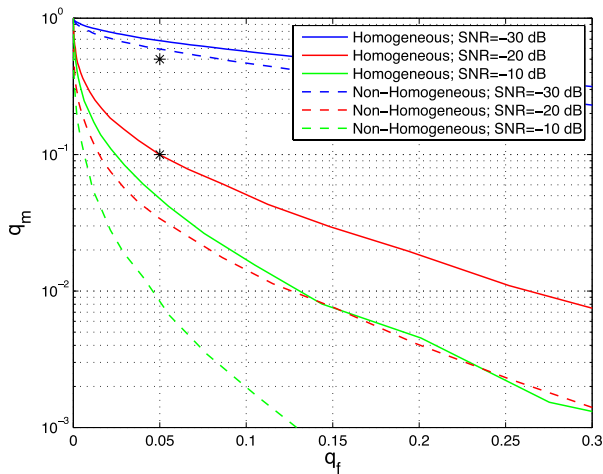


Fig. 13. Impact of the SNR on the CROC. Curves refer to a simulated scenario with  $K = 15$  transmitting sensors with pulse duration  $T_p = 1$  ms, each with  $(p_f = 0.05, p_m = 0.5)$  in the homogeneous scenario (solid lines) and 10 with  $(p_f = 0.05, p_m = 0.5)$  and 5 with  $(p_f = 0.05, p_m = 0.1)$  in the non-homogeneous scenario (dashed lines), and  $N = 1$  hydrophone at the fusion center, operating with sampling frequency  $f_s = 1$  kHz and integration time  $T_o = 10$  ms. The black asterisks (\*) represents the local sensing performance of the two types of considered sensor.

hydrophones at the fusion center, operating at  $\text{SNR} = -10$  dB with sampling frequency  $f_s = 2$  kHz.

It is apparent how the latter curve, corresponding to a realistic practical setup, almost achieves the former curve, i.e. the (ideal) observation bound. More specifically, the gap at  $q_f = 0.05$  is such that the realistic practical setup achieves  $q_m = 0.0084$  while the observation bound is  $q_m = 0.0035$ .

*Homogeneous vs. Non-Homogeneous Scenarios:* Finally, we consider the performance in a non-homogeneous scenario made of 10 sensors with default local performance and 5 sensors characterized by  $(p_f, p_m) = (0.05, 0.1)$ . Fig. 13 compares the CROC curves from the non-homogeneous scenario with those from the analogous homogeneous scenario considered in Fig. 2. The improvement due to the second group of (better performing) sensors is apparent, especially for large

TABLE II  
PERFORMANCE WITH ENERGY DETECTOR AND  $q_f = 0.05$

$N$	$K$	$f_s$	$T_o$	$T_p$	SNR	$p_f$	$p_m$	$q_m(\%)$
1	15	1 kHz	10 ms	1 ms	-20 dB	0.05	0.5	9.9
1	15	1 kHz	20 ms	1 ms	-20 dB	0.05	0.5	8.8
1	15	2 kHz	10 ms	0.5 ms	-20 dB	0.05	0.5	8.0
4	10	1 kHz	10 ms	1 ms	-20 dB	0.05	0.5	5.8
1	15	2 kHz	10 ms	1 ms	-20 dB	0.05	0.5	5.7
1	20	1 kHz	10 ms	1 ms	-20 dB	0.05	0.5	5.4
1	15	1 kHz	10 ms	1 ms	-10 dB	0.05	0.5	4.8
1	15	2 kHz	10 ms	2 ms	-20 dB	0.05	0.5	4.6
1	15	2 kHz	20 ms	1 ms	-20 dB	0.05	0.5	4.3
2	15	1 kHz	10 ms	1 ms	-20 dB	0.05	0.5	3.7
4	15	1 kHz	10 ms	1 ms	-20 dB	0.05	0.5	1.3
2	20	1 kHz	10 ms	1 ms	-20 dB	0.05	0.5	1.2
4	15	2 kHz	10 ms	1 ms	-10 dB	0.05	0.5	0.84
1	15	1 kHz	10 ms	1 ms	-20 dB	0.05	0.1	0.35
4	20	1 kHz	10 ms	1 ms	-20 dB	0.05	0.5	0.28
1	15	1 kHz	10 ms	1 ms	-20 dB	0.01	0.1	<0.01

SNR (indeed for large SNR sensing errors are dominate over reporting errors). In order to assess the benefit of the second group of sensors, it is worth noticing that replacing 5 sensors with local performance  $(p_f, p_m) = (0.05, 0.5)$  from the homogeneous scenario with 5 sensors with local performance  $(p_f, p_m) = (0.05, 0.1)$  in the case of  $\text{SNR} = -20$  dB and at a global probability of false alarm  $q_f = 0.05$  allows to reduce the global probability of missed detection from  $q_m = 0.099$  to  $q_m = 0.034$ .

Before concluding the paper, Tab. II highlights (with decreasing order) the performance in terms of global probability of missed detection ( $q_m$ ) of the presented configurations when a fixed global probability of false alarm  $q_f = 0.05$  is considered. More specifically, only those configurations achieving  $q_m < 0.10$  are listed. MIMO decision fusion based on energy detection, although suboptimal, is definitely an appealing strategy in underwater acoustic wireless sensor networks because on one hand is able to achieve extremely good performance on the other hands requires extremely low computational complexity and limited system knowledge. Additionally, it does not require any modification in order to deal with a non-homogeneous setup. It is worth remarking that

- the optimal choice for the integration time is depending on the specific acoustic environment, and is roughly  $T_o = \tau_\mu + 3\tau_{rms}$ ;
- the optimal choice for the pulse duration is depending on the frequency sampling,  $T_p = 1/f_s$ ;
- analytical characterization with respect to the number of sensors, the number of hydrophones, and local performance is difficult, however excellent performance (with small performance loss with respect to the optimal detector) may be achieved even with very low quality sensors and limited number of transmit/receive elements.

Although the quantitative results are linked to the specific values that were considered, we expect that the same qualitative results hold for a generic underwater environment.

## V. CONCLUSION

In this paper we considered a system for MIMO decision fusion in underwater sensor networks based on

energy detection. Underwater acoustic channels have been modeled with time-varying multipath and non-uniform Doppler shifts. Although not being optimal, the energy detector was selected for its low computational complexity and limited requirements on system knowledge. The impact on the performance of relevant design parameters has been analyzed and it has been shown how practical system setups may approach optimal performance in a realistic scenario even with low-quality sensors.

#### ACKNOWLEDGMENT

The authors would like to thank Dr. Y. Dong at the Shanghai Marine Electronic Equipment Research Institute, China, for comments and helpful discussions, and also the anonymous reviewers and the associate editor for their contribution to improve the quality of the manuscript.

#### REFERENCES

- [1] I. F. Akyildiz, D. Pompili, and T. Melodia, "Underwater acoustic sensor networks: Research challenges," *Ad Hoc Netw.*, vol. 3, no. 3, pp. 257–279, Mar. 2005.
- [2] J. A. Catipovic, "Performance limitations in underwater acoustic telemetry," *IEEE J. Ocean. Eng.*, vol. 15, no. 3, pp. 205–216, Jul. 1990.
- [3] L. Lanbo, Z. Shengli, and C. Jun-Hong, "Prospects and problems of wireless communication for underwater sensor networks," *Wireless Commun. Mobile Comput.*, vol. 8, no. 8, pp. 977–994, Oct. 2008.
- [4] D. B. Kilfoyle and A. B. Baggeroer, "The state of the art in underwater acoustic telemetry," *IEEE J. Ocean. Eng.*, vol. 25, no. 1, pp. 4–27, Jan. 2000.
- [5] P. A. van Walree and R. Otnes, "Ultrawideband underwater acoustic communication channels," *IEEE J. Ocean. Eng.*, vol. 38, no. 4, pp. 678–688, Oct. 2013.
- [6] P. Qarabaqi and M. Stojanovic, "Statistical characterization and computationally efficient modeling of a class of underwater acoustic communication channels," *IEEE J. Ocean. Eng.*, vol. 38, no. 4, pp. 701–717, Oct. 2013.
- [7] B. Li, S. Zhou, M. Stojanovic, L. Freitag, and P. Willett, "Multicarrier communication over underwater acoustic channels with nonuniform Doppler shifts," *IEEE J. Ocean. Eng.*, vol. 33, no. 2, pp. 198–209, Apr. 2008.
- [8] B. Li *et al.*, "MIMO-OFDM for high-rate underwater acoustic communications," *IEEE J. Ocean. Eng.*, vol. 34, no. 4, pp. 634–644, Oct. 2009.
- [9] Z. Wang, S. Zhou, G. B. Giannakis, C. R. Berger, and J. Huang, "Frequency-domain oversampling for zero-padded OFDM in underwater acoustic communications," *IEEE J. Ocean. Eng.*, vol. 37, no. 1, pp. 14–24, Jan. 2012.
- [10] P. A. van Walree and G. Leus, "Robust underwater telemetry with adaptive turbo multiband equalization," *IEEE J. Ocean. Eng.*, vol. 34, no. 4, pp. 645–655, Oct. 2009.
- [11] G. Zhang and H. Dong, "Spatial diversity in multichannel processing for underwater acoustic communications," *Ocean. Eng.*, vol. 38, nos. 14–15, pp. 1611–1623, Oct. 2011.
- [12] G. Zhang and H. Dong, "Experimental assessment of a multicarrier underwater acoustic communication system," *Appl. Acoust.*, vol. 72, no. 12, pp. 953–961, Dec. 2011.
- [13] G. Zhang and H. Dong, "Experimental demonstration of spread spectrum communication over long range multipath channels," *Appl. Acoust.*, vol. 73, no. 9, pp. 872–876, Sep. 2012.
- [14] S. Roy, T. Duman, L. Ghazikhanian, V. McDonald, J. Proakis, and J. Zeidler, "Enhanced underwater acoustic communication performance using space-time coding and processing," in *Proc. IEEE OCEANS Conf.*, vol. 1, Nov. 2004, pp. 26–33.
- [15] M. L. Nordenvaad and T. Oberg, "Iterative reception for acoustic underwater MIMO communications," in *Proc. IEEE OCEANS Conf.*, Sep. 2006, pp. 1–6.
- [16] D. B. Kilfoyle, J. C. Preisig, and A. B. Baggeroer, "Spatial modulation experiments in the underwater acoustic channel," *IEEE J. Ocean. Eng.*, vol. 30, no. 2, pp. 406–415, Apr. 2005.
- [17] T. C. Yang, "A study of spatial processing gain in underwater acoustic communications," *IEEE J. Ocean. Eng.*, vol. 32, no. 3, pp. 689–709, Jul. 2007.
- [18] E. M. Sozer, M. Stojanovic, and J. G. Proakis, "Underwater acoustic networks," *IEEE J. Ocean. Eng.*, vol. 25, no. 1, pp. 72–83, Jan. 2000.
- [19] D. Pompili, T. Melodia, and I. F. Akyildiz, "A CDMA-based medium access control for underwater acoustic sensor networks," *IEEE Trans. Wireless Commun.*, vol. 8, no. 4, pp. 1899–1909, Apr. 2009.
- [20] M. K. Park and V. Rodoplu, "UWAN-MAC: An energy-efficient MAC protocol for underwater acoustic wireless sensor networks," *IEEE J. Ocean. Eng.*, vol. 32, no. 3, pp. 710–720, Jul. 2007.
- [21] X. Guo, M. R. Frater, and M. J. Ryan, "Design of a propagation-delay-tolerant MAC protocol for underwater acoustic sensor networks," *IEEE J. Ocean. Eng.*, vol. 34, no. 2, pp. 170–180, Apr. 2009.
- [22] W.-H. Liao and C.-C. Huang, "SF-MAC: A spatially fair MAC protocol for underwater acoustic sensor networks," *IEEE Sensors J.*, vol. 12, no. 6, pp. 1686–1694, Jun. 2012.
- [23] G. A. Hollinger *et al.*, "Underwater data collection using robotic sensor networks," *IEEE J. Sel. Areas Commun.*, vol. 30, no. 5, pp. 899–911, Jun. 2012.
- [24] K. Baumgartner, S. Ferrari, and T. A. Wettergren, "Robust deployment of dynamic sensor networks for cooperative track detection," *IEEE Sensors J.*, vol. 9, no. 9, pp. 1029–1048, Sep. 2009.
- [25] M. Zorzi, P. Casari, N. Baldo, and A. F. Harris, "Energy-efficient routing schemes for underwater acoustic networks," *IEEE J. Sel. Areas Commun.*, vol. 26, no. 9, pp. 1754–1766, Dec. 2008.
- [26] Y.-S. Chen and Y.-W. Lin, "Mobicast routing protocol for underwater sensor networks," *IEEE Sensors J.*, vol. 13, no. 2, pp. 737–749, Feb. 2013.
- [27] S. Zhang, D. Li, and J. Chen, "A link-state based adaptive feedback routing for underwater acoustic sensor networks," *IEEE Sensors J.*, vol. 13, no. 11, pp. 4402–4412, Nov. 2013.
- [28] J. M. Jordet, M. Stojanovic, and M. Zorzi, "On joint frequency and power allocation in a cross-layer protocol for underwater acoustic networks," *IEEE J. Ocean. Eng.*, vol. 35, no. 4, pp. 936–947, Oct. 2010.
- [29] A. K. Mohapatra, N. Gautam, and R. L. Gibson, "Combined routing and node replacement in energy-efficient underwater sensor networks for seismic monitoring," *IEEE J. Ocean. Eng.*, vol. 38, no. 1, pp. 80–90, Jan. 2013.
- [30] B. Chen, R. Jiang, T. Kasetkasem, and P. K. Varshney, "Channel aware decision fusion in wireless sensor networks," *IEEE Trans. Signal Process.*, vol. 52, no. 12, pp. 3454–3458, Dec. 2004.
- [31] B. Chen, L. Tong, and P. K. Varshney, "Channel-aware distributed detection in wireless sensor networks," *IEEE Signal Process. Mag.*, vol. 23, no. 4, pp. 16–26, Jul. 2006.
- [32] J. Park, E. Kim, and K. Kim, "Large-signal robustness of the Chair-Varshney fusion rule under generalized-Gaussian noises," *IEEE Sensors J.*, vol. 10, no. 9, pp. 1438–1439, Sep. 2010.
- [33] A. Lei and R. Schober, "Coherent max-log decision fusion in wireless sensor networks," *IEEE Trans. Commun.*, vol. 58, no. 5, pp. 1327–1332, May 2010.
- [34] C. R. Berger, M. Guerriero, S. Zhou, and P. Willett, "PAC vs. MAC for decentralized detection using noncoherent modulation," *IEEE Trans. Signal Process.*, vol. 57, no. 9, pp. 3562–3575, Sep. 2009.
- [35] F. Li, J. S. Evans, and S. Dey, "Decision fusion over noncoherent fading multiaccess channels," *IEEE Trans. Signal Process.*, vol. 59, no. 9, pp. 4367–4380, Sep. 2011.
- [36] M. K. Banavar, A. D. Smith, C. Tepedelenlioglu, and A. Spanias, "On the effectiveness of multiple antennas in distributed detection over fading MACs," *IEEE Trans. Wireless Commun.*, vol. 11, no. 5, pp. 1744–1752, May 2012.
- [37] D. Ciuonzo, G. Romano, and P. Salvo Rossi, "Channel-aware decision fusion in distributed MIMO wireless sensor networks: Decode-and-fuse vs. decode-then-fuse," *IEEE Trans. Wireless Commun.*, vol. 11, no. 8, pp. 2976–2985, Aug. 2012.
- [38] D. Ciuonzo, G. Romano, and P. Salvo Rossi, "Performance analysis and design of maximum ratio combining in channel-aware MIMO decision fusion," *IEEE Trans. Wireless Commun.*, vol. 12, no. 9, pp. 4716–4728, Sep. 2013.
- [39] D. Ciuonzo, G. Romano, and P. Salvo Rossi, "Optimality of received energy in decision fusion over Rayleigh fading diversity MAC with non-identical sensors," *IEEE Trans. Signal Process.*, vol. 61, no. 1, pp. 22–27, Jan. 2013.

- [40] Z. Xu, J. Huang, and Q. Zhang, "Power constrained partially coherent distributed detection over fading multiaccess channels," *IEEE Sensors J.*, vol. 13, no. 7, pp. 2729–2736, Jul. 2013.
- [41] J. Lee and C. Tepedelenlioglu, "Distributed detection in coexisting large-scale sensor networks," *IEEE Sensors J.*, vol. 14, no. 4, pp. 1028–1034, Apr. 2014.
- [42] X. Song, P. Willett, J. Glaz, and S. Zhou, "Active detection with a barrier sensor network using a scan statistic," *IEEE J. Ocean. Eng.*, vol. 37, no. 1, pp. 66–74, Jan. 2012.
- [43] V. R. Kanchumathy, R. Viswanathan, and M. Madishetty, "Impact of channel errors on decentralized detection performance of wireless sensor networks: A study of binary modulations, Rayleigh-fading and non-fading channels, and fusion-combiners," *IEEE Trans. Signal Process.*, vol. 56, no. 5, pp. 1761–1769, May 2008.
- [44] S. M. Kay, *Fundamentals of Statistical Signal Processing: Detection Theory*, vol. 2. Englewood Cliffs, NJ, USA: Prentice-Hall, 1998.
- [45] P. K. Varshney, *Distributed Detection and Data Fusion*. New York, NY, USA: Springer-Verlag, 1996.
- [46] A. Goldsmith, *Wireless Communications*. Cambridge, U.K.: Cambridge Univ. Press, 2005.



**Pierluigi Salvo Rossi** (SM'11) was born in Naples, Italy, in 1977. He received the Laurea (*summa cum laude*) degree in telecommunications engineering and the Ph.D. degree in computer engineering from the University of Naples Federico II, Naples, in 2002 and 2005, respectively. During his Ph.D. study, he was a Researcher with the Inter-Departmental Research Center for Signals Analysis and Synthesis, University of Naples Federico II, the Department of Information Engineering, Second University of Naples, Aversa, Italy, and the Communications and Signal Processing Laboratory, Department of Electrical and Computer Engineering, Drexel University, Philadelphia, PA, USA, and an Adjunct Professor with the Faculty of Engineering, Second University of Naples. From 2005 to 2008, he held a post-doctoral position with the Department of Computer Science and Systems, University of Naples Federico II, the Department of Information Engineering, Second University of Naples, and the Department of Electronics and Telecommunications, Norwegian University of Science and Technology (NTNU), Trondheim, Norway, and visited the Department of Electrical and Information Technology at Lund University, Lund, Sweden.

He has been an Assistant Professor (tenured in 2011) of Telecommunications with the Department of Industrial and Information Engineering, Second University of Naples, and a Guest Researcher and Professor with the Department of Electronics and Telecommunications, NTNU, since 2008. He is an Editor of the *IEEE COMMUNICATIONS LETTERS*. His research interests fall within the areas of communications and signal processing.



**Domenico Ciunzio** (S'11–M'14) was born in Aversa, Italy, in 1985. He received the B.Sc. and M.Sc. (*summa cum laude*) degrees in computer engineering and the Ph.D. degree in electronic engineering from the Second University of Naples, Aversa, in 2007, 2009, and 2013, respectively. In 2011, he was involved in the Visiting Researcher Program at the Centre for Maritime Research and Experimentation, La Spezia, Italy, and worked in the Maritime Situation Awareness Project. In 2012, he was a Visiting Scholar with the Department of Electrical and Computer Engineering, University of Connecticut, Storrs, CT, USA. His research interests are mainly in the areas of data and decision fusion, statistical signal processing, target tracking, and probabilistic graphical models. He is a reviewer for several IEEE, Elsevier, and Wiley journals in the areas of communications, defense, and signal processing. He has also served as a reviewer and Technical Program Committee Member for several IEEE conferences.



**Torbjörn Ekman** (M'02) was born in Västerås, Sweden, in 1969. He received the M.Sc. degree in engineering physics and the Ph.D. degree in signal processing from Uppsala University, Uppsala, Sweden, in 1994 and 2002, respectively. In 2006, he joined the Department of Electronics and Telecommunications Norwegian University of Science and Technology (NTNU), Trondheim, Norway, as an Associate Professor. From 1997 to 1998, he was a Visiting Scientist with the Institute of Communications and Radio-Frequency Engineering, Vienna

University of Technology, Vienna, Austria, on a Marie Curie Grant. From 1999 to 2002, he visited the Digital Signal Processing Group at the University of Oslo, Oslo, Norway. From 2002 to 2005, he made his post-doctoral studies at the University Graduate Center, Kjeller, Norway. His current research interests include signal processing in wireless communications, scheduling of radio resources and dynamic modeling, and prediction of radio channels. He is currently participating in projects on broadband radio access and cognitive radio, and studying radio resource management and channel modeling.



**Hefeng Dong** received the B.Sc. and M.Sc. degrees in physics from Northeast Normal University, Changchun, China, in 1983 and 1986, respectively, and the Ph.D. degree in geoaoustics from Jilin University, Changchun, in 1994.

She was a Lecturer of Physics with Northeast Normal University, from 1986 to 1994, where she was also an Associate Professor from 1995 to 2000. She was a Visiting Scholar and Post-Doctoral Fellow with the Norwegian University of Science and Technology (NTNU), Trondheim, Norway, from 1999 to 2000 and 2000 to 2001, respectively. From 2001 to 2002, she was a Research Scientist with SINTEF Petroleum Research, Trondheim. Since 2002, she has been a Professor with NTNU. From 2008 to 2009, she was on a one-year sabbatical with the Underwater Acoustics Laboratory, University of Victoria, Victoria, BC, Canada. Her research interests include wave propagation modeling, geoaoustic inversion, and signal processing in ocean acoustics and seismics. She is a member of the Acoustical Society of America, the Norwegian Physical Society, and the Norwegian Acoustical Society.